Journal of Theoretical and Applied Information Technology
15th April 2026. Vol.104. No.7

ISSN: 1992-8645 www.jatit.org E-ISSN: 1817-3195

MODIFIED SHUFFLENET WITH TRANSFER LEARNING MODEL FOR BLOCKCHAIN ASSISTED SECURE LUNG CANCER CLASSIFICATION IN CLOUD-IOT ENVIRONMENT

AFFROSE[*1], ASHWANI KUMAR YADAV[2], AND ARCHEK PRAVEEN KUMAR[3], AND CHERUKU SANDESH KUMAR[4]

[*1]Research scholar, Department of Electronics and Communication Engineering, Amity University Rajasthan, Jaipur, Rajasthan 303002, India

[2,4]Assistant Professor, Department of Electronics and Communication Engineering, Amity University Rajasthan, Jaipur, Rajasthan 303002, India

[3]Professor, Department of Electronics and Communication Engineering, Gates Institute of Technology, Anantapuramu, Andhra Pradesh 515401, India

E-mail: [*1]roseaffrose557@gmail.com

ABSTRACT

Globally, lung cancer (LC) is the much prevalent source of cancer-based deceases. In recent years, classifying lung cancer using CT has become a new area of study in the area of medical image systems. A key factor in the LC diagnosis is the capacity to precisely determine the location and size of the disease. Rapid diagnosis, detection, classification, and evaluation of CT images are therefore necessary. The developed study is made to classify the LC using CT imageries. For classifying LC, the data (CT images) will be acquired from Cloud-IoT. The acquired data is stored in Blockchain to ensure its security. After acquiring the data, the LCC process begins by pre-processing the CT images using Processed Pixel-based Threshold-based Median Filtering (PPT-MF) technique. Subsequently, modified Res U-Net is used for segmenting the images. Then, features namely, Modified MRELBP, Local Monotonic Pattern (LMP), and PHOG are derived. After that, data augmentation is carried out using random sampling technique. Finally, classification is done using Transfer learning-based modified Shufflenet (TL-MSNet) model. From the analysis, a higher specificity of 98% is gained with TL-MSNet, whereas, existing methods score lower specificity values.

Keywords: *Lung cancer; PPT-MF Technique; Modified Res U-Net; Modified MRELBP; Modified Shufflenet.*

Nomenclature

Abbreviation	Description
AI	Artificial Intelligence
AP-RBN	Average Pooling Response Batch Normalization
BN	Batch Normalization
CT	Computed Tomography
CC	Cloud Computing
CAD	Computer-Aided Detection
CNN	Convolutional Neural Networks
CLAHE	Contrast Limited Adaptive Histogram Equalization
CADSS	Computer-Aided Decision Support System
DL	Deep Learning
DenseNet-201	Densely Linked Networks
3DDCNN	3d Deep Convolutional Neural Network
EHR	Electronic Health Record
ELTU	Exponential Linear Tanh Unit
ENN	Elman Neural Network
ECA	Effective Channel Attention Module
FPR	False Positive Rate
GF	Gaussian Filtering
iYOLOv5	Improved Yolov5
KNN	K-Nearest Neighbors
LMP	Local Monotonic Pattern
LCC	Lung Cancer Classification
LC	Lung Cancer
ML	Machine Learning
MRI	Magnetic Resonance Imaging
mAP	Mean Average Precision
mRPN	Multi-Region Proposal Networks
MRELBP	Median Robust Extended Local Binary Pattern
NSCLC	Non-SCLC
PPT-MF	Processed Pixel-based Threshold-based Median Filtering
PHOG	Pyramid of Histogram of Oriented Gradients
PHR	Personal Health Record
RF	Random Forest
ROI	Regions-of-Interest
SMA	Slime Mold Algorithm
SVM	Support Vector Machine
SCMO-MLL2C	Self-Upgraded Cat Mouse Optimizer with Machine Learning driven Lung

	Cancer Classification
SCLC	Small Cell Lung Cancer
SD	Standard Deviation
TL-MSNet	Transfer Learning-based Modified Shufflenet
TD	Training Data
WHO	World Health Organization's

1. INTRODUCTION

Cancer is said to be the major reason for millions of mortalities worldwide and it has turned out as a serious health issue among individuals [1] [2]. Cancer was ranked as the second major reason of fatality and as per WHO, it is expected that in 2020, 10 million fatalities occurred due to cancer. Cancer affects individuals of any age and it develops in any part of the human body. Cancer may be classified into over 100 distinct varieties, each with a unique set of traits and behaviors. Lung, colon, breast, stomach, and liver cancers are the most common types of cancer [3].[4] [5]. The lung cancer starts from the lungs, which are responsible for carrying out respiration. According to reports, LC claimed the lives of almost 1.80 million individuals in 2021. SCLC and NSCLC are the two wide kinds of LC [6] [7] [8] [9].

The LCC offers comprehensive knowledge regarding patient care perception, as various classes of lung tumors require distinct treatment modalities [10] [11] [12]. For identify the stage and type of LC, traditional Wetlab methods rely on visual evaluation of imaging data using certain standards, such as position and size of tumor. These approaches, however, are arbitrary and might lead to inter-observer variability. For overcoming this trouble, scholars have formed computer-based methods to automate the analysis of medical images for LCC [13] [14]. The development of automatic approaches for the exact interpretation of medical images, particularly the LCC, has been greatly aided by recent advances in AI. These methods enhance the efficacy of LCC and yield more accurate findings [15] [16] [17] [9].

Traditional medical imaging techniques for classifying and diagnosing LC include MRI and CT. Although MRI and CT images are the most often utilized image capture methods in medical imaging, each has unique properties and uses [16]. Nowadays, the detection of LC has been transformed by the usage of CT scans. Renowned for producing high-resolution images, CT scans are especially good at spotting tiny, calcified regions, which is essential for spotting LC in its early stages [9]. The use of CAD tools for LC diagnosis has augmented as a consequence of current advancements in ML and DL approaches [17] [18]. SVM, RF, and KNN are a few of the classic ML-based methods that have been used in the literature to help diagnose and categorize LC [19]. With these methods, features are manually extracted, which are deployed for training the classifiers. Moreover, handling the diverse functions is complicated and exhausting. Furthermore, the ML models are trained only with limited samples, which results in a generalization issue. Although DL models come in a variety of forms, CNNs are the much renowned ones for classifying tasks. Their hierarchical learning model of data makes it especially perfect for extracting complicated information from unprocessed input. Without human involvement, the CNN can automatically recognize and extract the most noticeable patterns. As long as the images have the same kinds of attributes, the CNN can successfully categorize them even if they differ greatly from the training samples. For CNNs to function well, a lot of data is necessary. In situations when obtaining a big dataset is difficult, this might be a problem.

Accordingly, the novel LCC approach comes up with below contributions.

- Proposes a new LCC model, where, pre-processing is performed using processed pixel-based threshold technique. Using PPT-MF method, the building up of noise and distortions in input CT image are avoided.
- Deploys modified ResU-Net for segmentation, where, the whole structure of existing Res U-Net is altered for enhancing the segmentation performance. Using modified ResU-Net, the network stability gets increased and segmentation could be done exactly
- Extracts new MRELBP features, where, the neighbor representation formula is modified based on proposed PPT-MF. Thus, it can captivate detailed features namely, macrostructure and microstructure information.
- Introduces TL-based Modified Shuffle Net, where, the TL-MSNet framework to be tested is allocated with pre-trained MSNet weights. Moreover, a new modified SNet is proposed with varied modifications.

The literature works on LCC are under in Section 2 Cloud-based data acquisition and blockchain- storage is under section 3. Section 4 and 5 describes proposed LCC framework and PPT-MF-based pre-processing. Section 6 describes modified Res U-Net. Modified features and data

augmentation are explained in section 7. TL-MSNet is demonstrated in Section 8. Section 9 and 10 describes result and conclusion.

2. LITERATURE REVIEW

2.1 Related works

Lung-EffNet was a new TL-based predictor for LCC that was suggested by Rehan *et al.* [9] in 2023. The design of EfficientNet served as the foundation for Lung-EffNet. Five EfficientNet variations, B0–B4, were used to assess Lung-EffNet. The IQ-OTH/NCCD dataset for LC patient based upon the existence or absence of LC was used for analysis. In order to overcome the biases, the problem of class imbalance was addressed using a variety of data augmentation techniques. The expected results showed that Lung-EffNet, which was based on EfficientNetB1, performed better than other CNNs.

The use of DL techniques, including Faster R-CNN, YOLOv5, and a suggested iYOLOv5, for lung nodule detection was investigated by Harale *et al.* [20] in 2024. The models were trained to reliably identify lung nodules using the LIDC-IDRI dataset. With a remarkable mAP, the suggested iYOLOv5 model outperformed the baseline models. These results highlighted the iYOLOv5 model's potential to enhance lung nodule identification and classification, which increased the precision of medical imaging diagnostics.

In 2023, Mahum and Salman [21] offered Lung-RetinaNet, a new approach for LCC. In order to rise the degree of semantics, a feature fusion method was created to combine different layers of network. Moreover, the contextual module deployed a streamlined and light weighted method for integrating context data with single layer in order to enhance features and locate the small tumors efficiently. The proposed model was compared with the most advanced DL-based techniques.

A new CADSS for LCC that employed a 3DDCNN was developed by Anum *et al.* [19] in 2020. When radiologists were making decisions about LC diagnosis, this decision support technology gave them a second viewpoint. mRPN was utilized for automated identification of possible ROI and median intensity projection to take advantage of 3-D data gathered via CT images. This demonstrated the potential of DL in conjunction with CC for precise and effective lung nodule diagnosis using CT imaging, which aided medical professionals and radiologists in the treatment of patients with LC.

In 2024, Nahed *et al.* [22] sought to improve CAD systems' efficacy using a variety of techniques. First, CT scans were preprocessed using CLAHE technique to enhance their visual quality. By combining the CLAHE approach with various optimization techniques, more refinement was accomplished. The performance of suggested model was improved by applying the CutMix data enrichment approach. The efficiency of these designs in classification tasks was assessed in the study without or with the CLAHE method being used. The study's empirical results showed a notable decrease in the FPR and a general boost in diagnostic precision.

A novel SCMO-MLL2C method was introduced by Ragab *et al.* [23] in 2023 for use with CT scans. The primary goal of the proposed SCMO-MLL2C system was to identify and categorize CT scans into three groups: normal, malignant, and benign. GF was the method used by the SCMO-MLL2C technique to remove noise from the CT images. Additionally, the SMA was used as a parameter enhancer in the feature extraction process using DenseNet. In this work, LC was classified using the ENN method, which was optimized using SCMO.

In 2024, Wehbe *et al.* [24] provided a sophisticated technique for classifying and detecting LC subtypes utilizing the most recent YOLO version, specifically designed for CT image processing. Early and precise diagnosis was essential for efficient treatment planning, especially in light of the rising death rates linked to lung cancer. To accurately identify and categorize different forms of LC, the suggested technique uses single-shot object identification. The efficiency of developed model was demonstrated by the experimental outcomes, which showed an exceptional mAP of 97%.

In 2023, Naseer *et al.* [25] sought to use AI approaches to create automated methods for correctly detecting and categorizing LC via CT images. Segmentation of lobe, extracting candidate nodules, and classification of nodules were commonly included in the procedure. The modified U-Net scheme was used in the suggested LCC. The first step used a CT slice and a modified U-Net architecture to segment the lobe, and the second phase used an improved U-Net for extracting the nodule. In the third step, improved AlexNet was deployed and SVM was used to classify LC.

In 2025, Kalidindi *et al.* [26] has suggested a safe and effective strategy for detecting lung cancer. First, many benchmark datasets are used to gather CT scan data. Smart contracts within the blockchain network guarantee security and anonymity during data exchange, allowing

decentralized and impenetrable data management. A new hybrid ensemble deep learning model called Hybrid Convolutional Neural Network with Autoencoder and Long Short-Term Memory (HCNN-ALSTM) is used to diagnose lung cancer. The HCNN-ALSTM method effectively extracts features from CT images by using Autoencoder and LSTM. Additionally, the Modified Krill Herd Algorithm (MKHA), a heuristic optimization technique, optimizes its parameters.

2.2 Problem Statement

Existing methods primarily rely on centralized cloud-based data storage, which raises serious concerns regarding data privacy, integrity, and unauthorized access to sensitive CT images and Electronic Health Records. Conventional preprocessing techniques such as Gaussian, mean, and standard median filtering are ineffective under high-density noise conditions and often degrade important diagnostic details. Widely used segmentation models, including U-Net and Res U-Net, suffer from contextual information loss, pixel-class imbalance, and limited depth representation, leading to inaccurate tumor boundary detection. Lightweight CNN models such as ShuffleNet, although computationally efficient, are limited in capturing fine-grained lung cancer patterns due to aggressive channel reduction and heavy reliance on group convolutions. In addition, most existing LCC frameworks focus solely on classification accuracy and ignore secure data management and end-to-end system integration. To address these limitations, this work proposes a blockchain-assisted, Cloud–IoT-based LCC framework that integrates robust noise-resistant preprocessing, modified Res U-Net segmentation, enhanced feature extraction, and a transfer learning-based Modified ShuffleNet (TL-MSNet), thereby achieving secure data handling, improved segmentation accuracy, and high classification performance with reduced computational complexity.

3. CLOUD-BASED HEALTH DATA ACQUISITION AND BLOCKCHAIN-BASED STORAGE

3.1 Cloud-based Health Data Acquisition

An EHR is a collection of patient data. The PHR contains data related to individual medical care. These data are obtained from devices like sensors that patients wear [27]. Patients may grant medical personnel access of their PHR data to medical professionals. The aim of EHR mechanism is to protect privacy and accessibility while optimizing the safety of stored data. As EHR maintains enormous volumes of data, it is very helpful for ML and data analytics. It is therefore crucial for future investigations aimed at disease prediction. The EHR and PHR are then uploaded to cloud by healthcare professionals, which can be assessed whenever necessary. Additionally, it facilitates healthcare monitoring and individualized healthcare services.

Here, the acquired data from cloud is stored using block chain technology.

3.2 Blockchain Storage

Blockchain technology is used to store patient data on the cloud. EHR was a popular use case for blockchain appliances in the healthcare sector [28]. The blockchain technology provides distributed ledger system, which is a new alternative to traditional data management techniques that depend on external cloud services. Security concerns about EHR may be resolved using this technology. Particularly, in PHR applications, blockchain has decentralized control and integrate incentive systems via smart contracting that can further promote their widespread usage. These benefits have inspired the use of blockchain technology for data storage. Fig. 1 shows the architecture of cloud-oriented healthcare system.

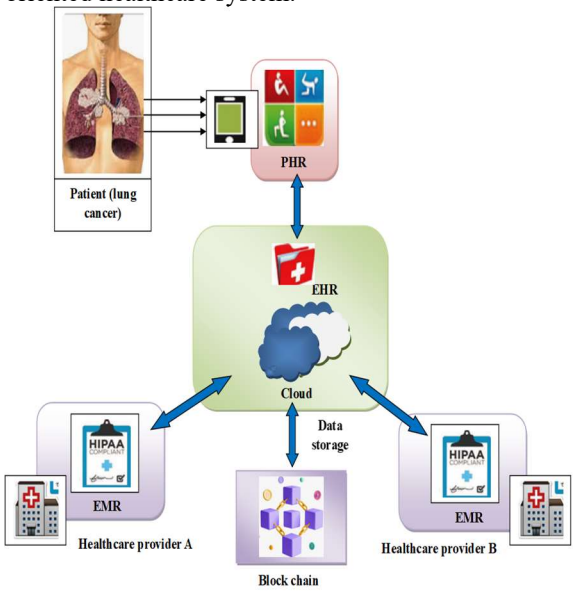

Figure 1: Framework showing cloud-oriented healthcare system

3.3. Proposed Lung Cancer Classification Framework

The data (CT image) is acquired from block chain and used for LCC analysis. During LCC, the below processes are carried out.

(i) At first, preprocessing is done using PPT-based MF technique.

(ii) Segmentation is made by means of Modified Res U-Net model.

(iii) Then, the features like modified MRELBP, LMP and PHOG are derived.

(iv) Subsequently, data augmentation is done using random sampling technique.

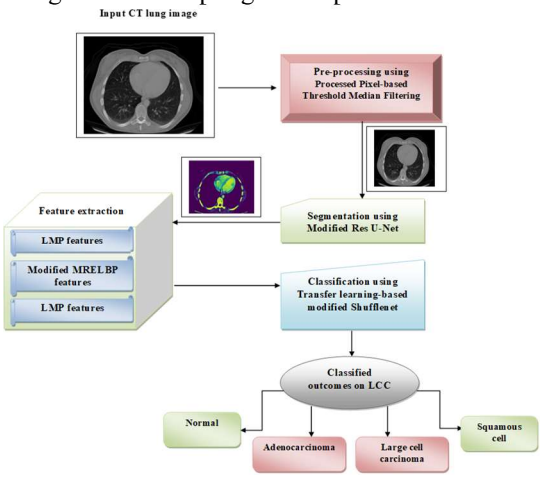

Figure 2: Framework for developed LCC model

3.3.1. Pre-Processing via Processed Pixel-Based Threshold Method

The input lung CT images, denoted as (IL) is preprocessed in order to standardize the medical images and minimize imaging artifacts. Here, the acquired CT lung image IL is preprocessed via PPT-based MF method.

PPT-based MF method: It [29] is a method of replacing each pixel value in a given kernel with the median of the pixel adjacent to it. The MF output is expressed as in Eq. (1), where, $G(z,u)$ indicates the noise in IL. k is the kernel positioned at the pixel (z,u). The MF effectively reduces noise while preserving important aspects of the image.

$$IL^{P} = med\left\{G(z,u),(z,u)\in k_{u,v}\right\} \quad (1)$$

Even though MF reduce noise, it is effective only if the noise is impulse noise, such with salt and pepper. When there is more than 20% noise or a high spatial density of noise, they perform poorly. Furthermore, a high kernel size may result in improper image smoothing and blurring of important information.

Therefore, a new MF method is proposed based on processed pixel-based threshold technique.

The steps followed for proposed PPT-based MF method is mentioned below.

(v) Finally, classification is done using TL-MSNet model and classified outcomes such as normal, adenocarcinoma, large cell carcinoma and squamous cell carcinoma are obtained.

Fig. 2 displays the framework of developed LCC work.

A 2D window with dimension 3×3 is chosen and positioned near the processed pixel, $P(z,u)$ in damaged image.

In the chosen window, the pixels are sorted based on ascending order. Then, median value of pixel $\left(P_{me}\right)$, maximum $\left(P_{max}\right)$ and minimum values of pixel $\left(P_{\min}\right)$ of sorted vector V_0 are determined.

Then, Markov blox blur filter is applied on the input IL, and new filtered image is obtained as shown in Eq. (2).

$$MBBF = \left[Y(z,u)+\delta(I,J)\right]/2 \quad (2)$$

For novel filtered image, find median $\left(f_{me}\right)$, maximum $\left(f_{max}\right)$ and minimum values of pixel $\left(f_{\min}\right)$.

Compute a novel value of pixel for $P(z,u)$ in the damaged image as given in Eq. (3).

$$Y' = \frac{\left\{\left[\left(P_{\min}+f_{\min}\right)*\frac{1}{1+\exp\left(f_{me}\right)}\right]*P_{\max}\right\} - \left\{\left[\left(P_{\max}+f_{\max}\right)*\frac{1}{1+\exp\left(P_{me}\right)}\right]*P_{\min}\right\}}{\left[\max\left(\left(\frac{\left|P_{\max}+f_{\min}\right|}{P_{me}}\right),\left(\frac{\left|P_{\min}+f_{\max}\right|}{f_{me}}\right)\right)\right]} \quad (3)$$

If the processed value of pixel $(Y')\geq T$, it is determined as uncorrupted and remains unchanged. Else, it is determined as corrupted. The threshold, T is formulated as given in Eq. (4).

$$T = \frac{2}{m}\sum_{i=\frac{m}{4}+1}^{\frac{3m}{4}} Y' \quad (4)$$

Thus, using processed pixel-based threshold method, the building up of noise and distortions in input CT image can be avoided. In addition, the undesired variations on the input CT image can be eliminated during processed pixel-based threshold technique. Moreover, the image will be scaled to a

normal range and it is made simpler for handling and comparing the difference in intensity.

The pre-processed image using processed pixel-based threshold method is signified as IL^{PPT} .

3.3.2. Segmentation using Modified Res U-Net

Res U-Net comprises of an encoder and decoder structure and is employed widely for segmenting images [30]. It is an improved form of U-Net architecture. A bridge joins the encoder and decoder to form the Res U- Net. The Res U-Net uses a gateway, an encoding connection, and a decoding mechanism to link different networks. 2 (3 × 3) conv with ReLU activation as well as pre-activated residual block are included in Res U-Net as seen in Fig. 3.

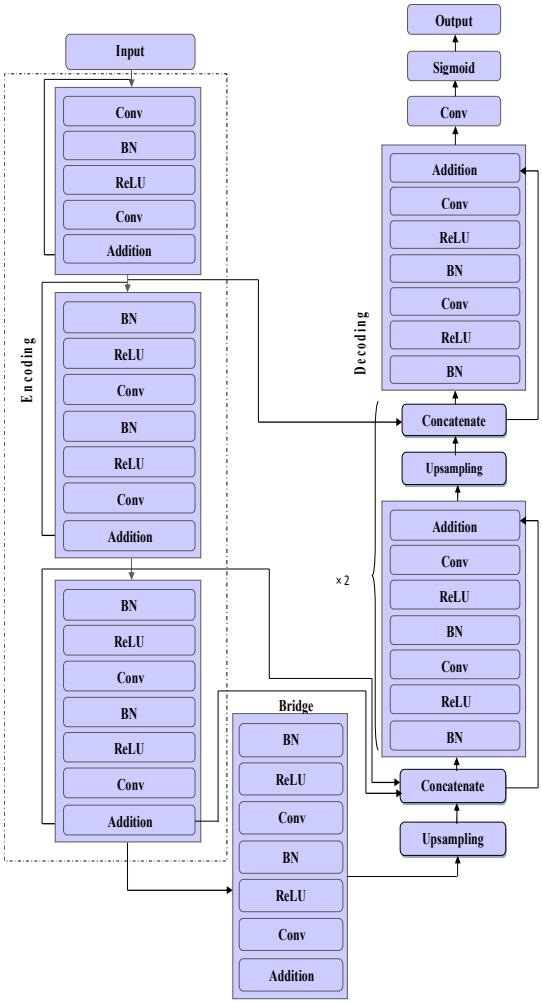

Figure 3: Conventional Res U-Net

Even though conventional Res U-Net resulted in better segmentation, it results in contextual info loss and it could not learn more complex and deep representations that is essential for segmenting images. Furthermore, in conventional Res U-Net, pixel imbalances occur, in which some pixel class seems to appear much frequent, which might affect the efficacy of the network adversely. The modified Res U-Net solves these problems by deploying new layers with change in structure.

According to modified Res U-Net, the whole structure of Res U-Net is altered for enhancing the segmentation performance. Here, new layers namely, Leaky ReLU, proposed residual block, Transpose conv and softmax layers are employed.

The existing residual block contains 2 conv layers and a ReLU layer. In modified Res U-Net, the proposed residual block is incorporated with new layers like BN, ELTU, Leaky ReLU instead of ReLU and conv 2D functions. The new residual block is illustrated in Fig. 4.

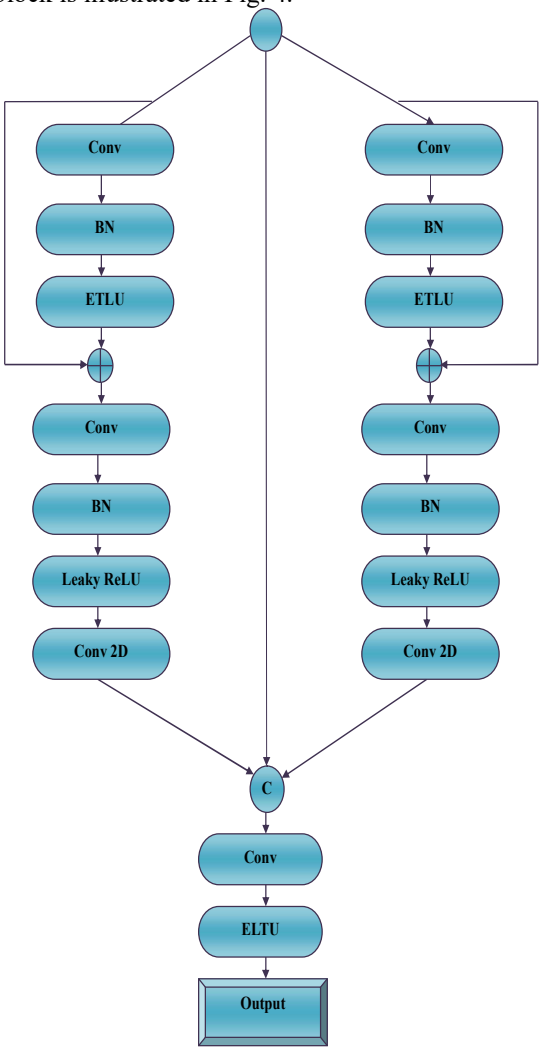

Figure 4: Proposed Residual block

The ELTU function in proposed residual block is formulated in Eq. (5), wherein, y is the output from prior layer and β is a parameter with value 1.0.

$$ELTU = \begin{cases} \left[y + \left(\frac{e^{y} - e^{-y}}{e^{y} + e^{-y}} \right) \right] \Big/ 2, & y > 0 \\ \left(\beta \exp(y) - 1 \right), & if\ y \le 0 \end{cases} \quad (5)$$

The modified Res U-Net enhances the generalization ability and improves the efficacy of representing learning features at varied depth levels. Also, it retains the significant contextual info throughout segmenting process. In addition, the network stability gets increased and segmentation could be done exactly. The modified Res U-Net structure is revealed in Fig. 5. The segmented lung image is indicated by IL^{S}.

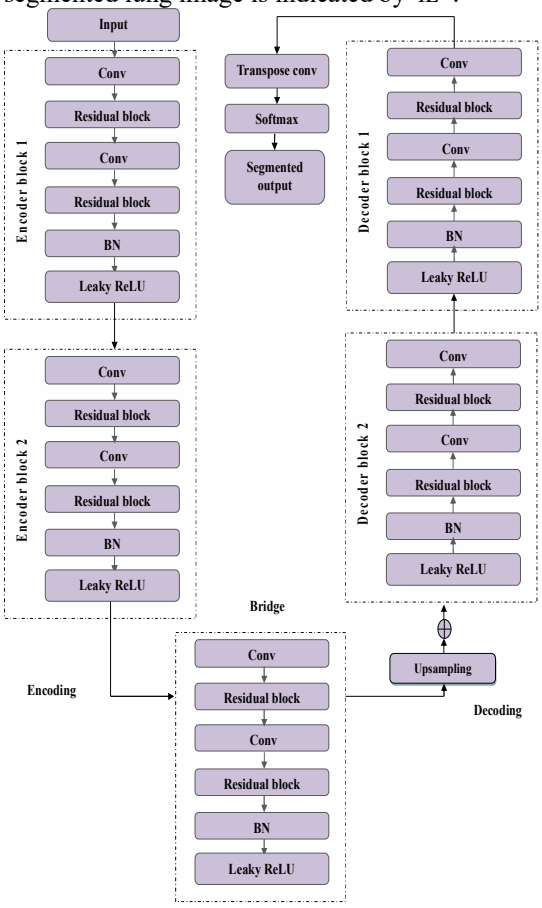

Figure 5: Modified Res U-Net Architecture

3.4. Modified Features and Data Augmentation

3.4.1 Feature extraction

The feature is a piece of information pertaining to the image content; in simple terms, it determines if a certain region of the image contains certain attributes. The following features are derived from IL^{S}:

- PHOG features
- Local monotonic pattern and
- Modified MRELBP

PHOG features [31]: PHOG is used to retrieve the spatial patterns of shapes in IL^{S}. This method first divides IL^{S} into regions using spatial pyramid matching at different resolutions. Subsequently, IL^{S} is fragmented into fine spatial grids, repeating the doubling of the number of divisions in each axis direction. The gradients are computed to extract PHOG features from IL^{S}. With this method, the grayscale image must be filtered with filter kernels like $Q_{U} = [-1\ 0\ 1]$ and $Q_{V} = \begin{bmatrix} 1 \\ 0 \\ -1 \end{bmatrix}$, and the derivatives of U and V are determined by convolution operations as $a_{U} = I * Q_{U}$ *and* $a_{V} = I * Q_{V}$ .. Eq. (6) and (7) are used to assess the gradient's size and direction.

$$a_{G} = \sqrt{\left(a_{U}^{\ 2} + a_{V}^{\ 2} \right)} \quad (6)$$

$$a_{O} = \arctan \frac{a_{V}}{a_{U}} \quad (7)$$

LMP [32]: This operator is used in an attempt to utilize bigger micro patterns composed of pixels at different radii. It preserves micro-patterns by considering monotonic intensity fluctuations in a single direction for creating a binary pattern for middle pixel. This procedure is comparable to LBP. Equation (8) is used to determine LMP for IL^{S}.

$$LMP_{\left(\Psi_{c}, \chi_{c}\right)} = \sum_{o=0}^{o-1} s\left(R_{o1} - R_{c} \right) \wedge s\left(R_{o2} - R_{o1} \right) * 2^{o} \quad (8)$$

In Eq. (8) R_{c} signifies intensity of center pixel $\left(\Psi_{c}, \chi_{c}\right)$; R_{o1} and R_{o2} signifies intensity values of o equally positioned pixels.

Modified MRELBP: MRELBP [33] is the modified version of ELBP descriptor, wherein, the intensities of distinct pixel are substituted by a median filter response $\varphi(\ )$. For a median filter φ and center pixel g_{c}, the MRELBP-CI, MRELBP-NI and MRELBP-RD descriptors are described as below:

Representation of center pixel: Eq. (9) shows the formula of deploying $\varphi(\ )$ to $G_{c,v}$, the local

patch of dimension $w \times w$ positioned at $\varphi\left(G_{c,v}\right)$, and η_v signifying the mean of $\varphi\left(G_{c,v}\right)$ on IL^S.

$$MRELBP-CI_{p,r}\left(g_c\right)=S\left(\varphi\left(IL^S_{c,w}\right)-\eta_w\right) \quad (9)$$

Representation of Neighbor: It is well-defined in Eq. (9), wherein, $G_{p,r,w_p,m}$ refers to a patch of dimension $w_p \times w_p$ positioned on $g_{p,r,m}$, r refers to neighbor pixels, p refers to radius, $S(.)$ refers to sign function.

$$MRELBP-NI_{p,r}\left(g_c\right)=\sum_{m=0}^{r-1}S\left(\varphi\left(IL^S_{p,r,w_p,m}\right)-\eta_{p,r,w_p}\right)2^m \quad (9)$$

$$\eta_{p,r,w_p}=\frac{1}{r}\sum_{m=0}^{r-1}\varphi\left(IL^S_{p,r,w_p,m}\right) \quad (10)$$

Representation of radial variance: It is defined in Eq. (11), wherein, $IL^S_{p,r,w_p,m}$ and $IL^S_{p-1,r,w_{p-1},m}$ signify the patches positioned at the adjacent pixels $g_{p,r,m}$ and $g_{p-1,r,m}$ correspondingly.

$$MRELBP-RD_{p,p-1,r,w_p,w_{p-1}}\left(g_c\right)= \sum_{m=0}^{r-1}S\left(\varphi\left(IL^S_{p,r,w_p,m}\right)-\varphi\left(IL^S_{p-1,r,w_{p-1},m}\right)\right)2^m \quad (11)$$

Although conventional MRELBP discovers spatial info, it could not captivate details regarding macrostructure. In homogenous or much smoother areas, the existing MRELBP fails to captivate subtle info, which leads to minimal discriminatory power of specified texture.

Thereby, a new formulation is proposed for prevailing over the existing issues of MRELBP. Here, the neighbor representation in Eq. (9) and (10) are modified as shown in Eq. (12) and (13), where, β = 0.6. particularly, the PPT-based MF method used in pre-processing step is used for computing φ,

$$MRELBP-NI_{p,r}\left(g_c\right)_{new}=\sum_{m=0}^{r=1}\left(\frac{\sqrt{\left(\left|S\left(\varphi\left(IL^S_{p,r,w_p,m}\right)\right)\right|-\left|\eta_{p,r,w_p}\right|\right)^2}}{\min\left(\sqrt{\sum_{m=0}^{r-1}\left[S\left(\varphi\left(IL^S_{p,r,w_p,m}\right)\right)\right]^2},\sqrt{\sum_{m=0}^{r-1}\left[\eta_{p,r,w_p}\right]^2}\right)}+\beta\right) \quad (12)$$

$$\eta_{p,r,w_p}=\frac{\left[\sum_{m=0}^{r-1}\left(\varphi\left(IL^S_{p,r,w_p,m}\right)\right)^2\right]}{\left[\sum_{m=0}^{r-1}\left(\varphi\left(IL^S_{p,r,w_p,m}\right)\right)\right]} \quad (13)$$

The proposed $MRELBP-NI_{p,r}\left(g_c\right)_{new}$ enhances the performance of existing MRELBP in extracting fine features from IL^S. In MRELBP, the individual intensities of pixels are replaced at a point with specified representation upon an area. Thus, it can captivate detailed features namely, macrostructure and microstructure information.

The entire features are represented as Γe, $\Gamma e=\left[MRELBP_{new}+PHOG+LMP\right]$, which are then subjected to data augmentation. The symbols and its description are tabulated in Table 1.

Table:1 Notation List

Symbol	Description
IL	Input lung CT image
k	kernel positioned at the pixel
T	Threshold
y	Output
β	parameter
IL^S	segmented lung image
R_c	intensity of center pixel
μ_B	mean of Υ_i
σ_B	Standard Deviation of Υ_i.
IL^D	data augmented lung feature
$S(.)$	sign function
p	radius

3.4.2 Data Augmentation

Data augmentation is an approach that artificially expands the training set by making sample copies of an existing dataset. It involves applying small adjustments to the dataset or using DL for creating new data samples. Here, random sampling technique [34] is used to augment the feature set Γe.

A subset of a population chosen at random is known as a simple random sample. Each component of the sample has an exact equal probability of getting chosen using this sampling technique. As it only takes single random selection and minimal prior population knowledge, this approach is the simplest of all probability sampling techniques. Any study conducted on this sample must have high external and internal validity and be

less susceptible to research flaws like sampling bias and selection bias since it employs randomization.

The data augmented lung features are indicated as IL^D.

3.5 Classification of Lung Cancer using Modified ShuffleNet with Transfer Learning

The augmented features $\left(IL^D\right)$ is passed to TL-MSNet for LCC. In fact, the TL-MSNet framework is allocated with pre-trained MSNet weights. The network is trained for a specified task and then reutilized for an associated another task. Here, MSNet is pre-trained and a weight is attained. The same weight is applied to MSNet while testing. The MSNet is examined using Chest CT-Scan images Dataset that gives outputs on "0 - normal, 1 - adenocarcinoma, 2 – large cell carcinoma, 3 – squamous cell carcinoma".

3.5.1 TL-based Modified Shufflenet

A ML technique known as TL includes training the network for a purpose and then utilizing it again for another related function. Here, the MSNet model is trained with augmented features, whose output will be the weight. This weight as well as augmented features $\left(IL^D\right)$ are then applied to another MSNet during testing process. This saves the execution time of the classification process.

A compact CNN design called Shuffle Net [35] was created to operate effectively on mobile devices. It reduces computation without compromising accuracy by enhancing group convolution performance through the use of channel shuffling operations. Shuffle Net is used in the classification stage to categorize the characteristics that have been retrieved from images of lung cancer.

Shuffle Net uses two primary tactics:

1. Group Convolution: This lowers the calculation and parameter count needed.
2. Channel Shuffle: This enhances feature learning and model accuracy by enabling the model to effectively mix data from several channels.

However, in existing SNet, the accurateness of visual task is minimized and the computing complexity of the network will be increased, which is a crucial issue to be resolved. Furthermore, SNet may not be able to capture subtle and detailed properties that are essential for accurate LCC due to to its severe channel reduction and dependence on group convolutions. This makes it more difficult for the model to identify fine-grained characteristics, particularly when analyzing complicated patterns in images of lung cancer.

Modified Shuffle Net: To overcome the above-said failings, a new modified SNet is proposed with diverse alterations. The MSNet involves new layers namely, Ghost module, proposed AP-RBN, proposed ECA, average and maximum pooling and flatten layer. Here, 4 Ghost modules are included and 2 proposed AP-RBN layers with DW conv are included.

Ghost Module: It is a method for network compression. Compared to regular convolution, this module improves network performance by lessening the network processing and parameters while preserving the accuracy [36].

Proposed ECA: The attention processes highlight particularly on the important information. It continually adjusts the weight to allow the election of significant info under dissimilar conditions, ignoring the low-weight insignificant data [36]. However, to speculate more deeply about the model's complexity, we propose a new ECA structure as given in Fig. 6. The ECA that comprises layers like average pooling, 1×1 DW conv, 1×1 conv, feature map and 1D conv.

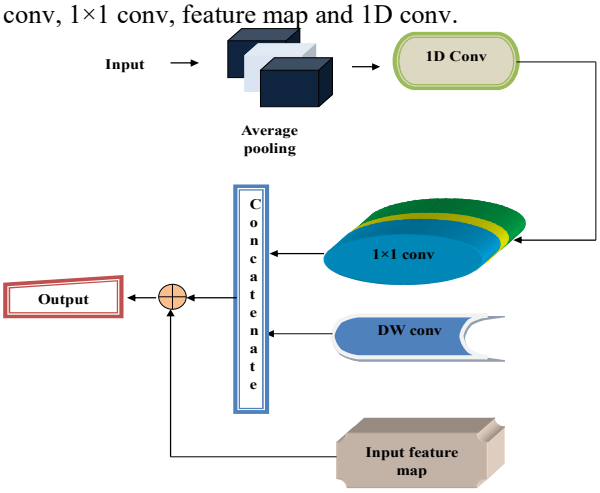

Figure 6: Proposed ECA architecture

Proposed AP-RBN: The proposed AP-RBN is computed based on BN and average pooling formulations. The average pooling formulation is in Eq. (14), wherein, d_i implies feature value in pooling area H_j and λ=1.

$$A_j = (1-\lambda)\frac{1}{|H_j|}\sum_{i\in H_j} d_i \quad (14)$$

The proposed AP-RBN is formulated based on A_j as given in Eq. (15), where, μ_B points out mean of Υ_i and σ_B points out the SD of Υ_i.

$$AP-RBN_j = \left\{ \left[\frac{\left(\Upsilon_i * A_j\right) - \mu_B}{\left(\sqrt{\sigma_B^2 + \varepsilon}\right) * A_j} \right] + \left[\frac{\Upsilon_i - \left(\mu_B * A_j\right)}{\sqrt{\sigma_B^2 + A_j}} \right] \right\} \quad (15)$$

The TL-MSNet overcomes the computing complexity issues and accuracy issues in existing SNet using the AP-RBN technique. The AP-RBN technique leads the network in light weighted path. Moreover, it sustains a better balancing among the accuracy and running speed of the network. Further, the computing complexity of the existing SNet model is reduced using proposed TL-MSNet classifier. The TL-MSNet gives outputs on "0 - normal, 1 - adenocarcinoma, 2 – large cell carcinoma, 3 – squamous cell carcinoma".

Fig. 7 represents the TL-MSNet architecture. The hyperparameter of classifiers are tabulated in Table 2.

Table 2: Hyperparameters of classifiers

Classifier	Hyper parameter
Improved Shuffle Net classifier	Optimizer – Adam
	Loss – Categorical crossentropy
	Metrics – accuracy
	Batchsize-1000
	Epochs – 50
Improved ResNet segmentation	Optimizer – adam
	Loss – binary_crossentropy
	Batchsize-16
	Epochs-50

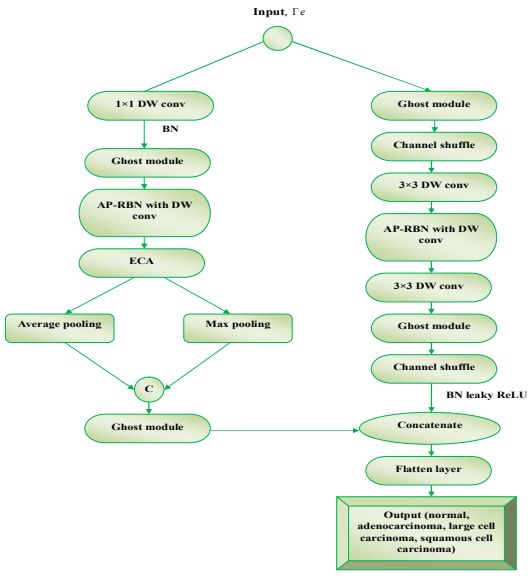

Figure 7: Architecture of Proposed TL-MSNet

4. RESULTS AND DISCUSSION

4.1 Simulation procedure

The developed TL-MSNet scheme for LCC was implemented in PYTHON. "In addition, we run the simulation on a system equipped with 64-bit OS, x64 based processor and had 16.0 GB (13.9 GB usable) of RAM". The assessment was made for TL-MSNet over Lenet, shuffle net, squeeze net, Link Net, alexnet, Efficient Net [9] and Dense Net [37]. The data to analyse the developed work was attained using "Chest CT-Scan images Dataset [38].

Dataset description: The dataset used in this study consists of 1,000 lung CT images categorized into four classes: normal (Class 0), adenocarcinoma (Class 1), large cell carcinoma (Class 2), and squamous cell carcinoma (Class 3). The class-wise distribution of the original dataset includes 215 normal images, 338 adenocarcinoma images, 187 large cell carcinoma images, and 260 squamous cell carcinoma images. To address class imbalance and enhance model generalization, data augmentation was performed, increasing the dataset size to 3,000 images. After augmentation, the class distribution became 645 normal, 1,014 adenocarcinoma, 561 large cell carcinoma, and 780 squamous cell carcinoma images.

For performance evaluation, the augmented dataset was partitioned using multiple train–validation–test split ratios to assess the robustness of the proposed model. Specifically, training proportions of 60%, 70%, 80%, and 90% were considered. For the 60% split, 1,440 images were used for training, 360 for validation, and 1,200 for testing. For the 70% split, 1,680 images were allocated for training, 420 for validation, and 900 for testing. Similarly, the 80% split consisted of 1,920 training images, 480 validation images, and 600 testing images, while the 90% split employed 2,160 images for training, 540 for validation, and 300 for testing. These varied split configurations ensure comprehensive evaluation and reliable performance assessment of the proposed lung cancer classification framework. The sample images showing lung cancer are given in Fig. 8.

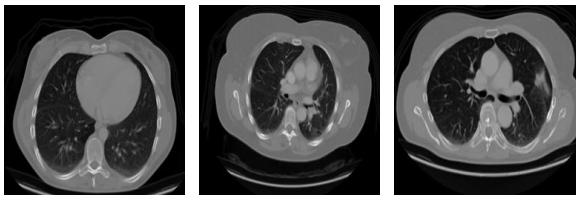

(a) (b) (c)

Figure 8: Illustration of original samples

4.2 Analysis on Pre-processing

The pre-processing analysis for LCC using proposed PPT-MF over existing techniques is exhibited in Fig. 9. For better LCC, the images utilized should be accurately pre-processed. On distinguishing over conventional MF, GF and mean filters, proposed PPT-WF shows images with accurate resolution as shown in Fig. 9. As we proposed a new MF method based on processed pixel-based threshold technique, the building up of noise and distortions in input CT image can be avoided. In addition, the undesired variations in the CT image can be eliminated during processed pixel-based threshold technique. It is further established from SSIM and PSNR study in Table 3. The PSNR and SSIM obtained via PPT-MF is higher about 36.176 and 0.9398 correspondingly. While, conventional MF, GF and mean filters attains less PSNR and SSIM values.

Input image

MF

Gaussian blur image

Mean filter

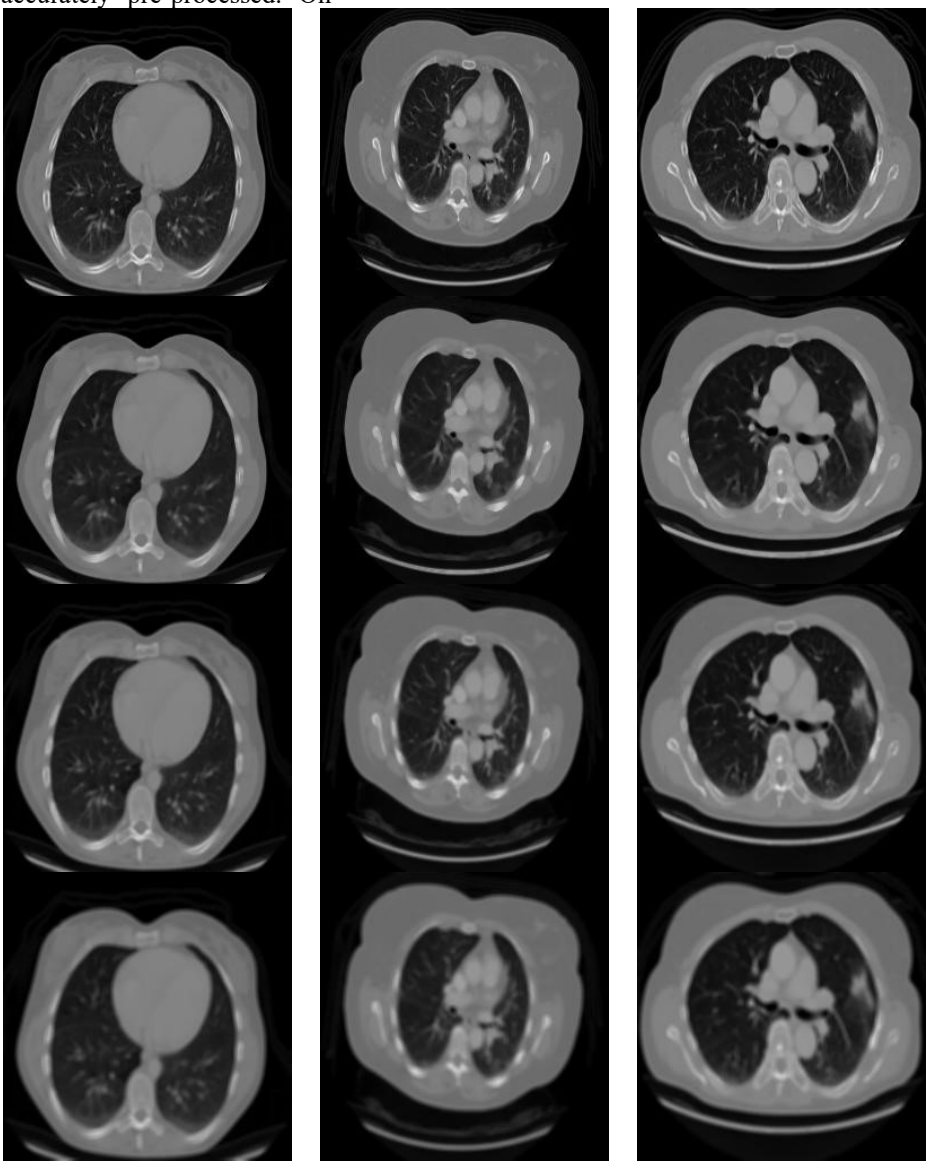

PPT-MF

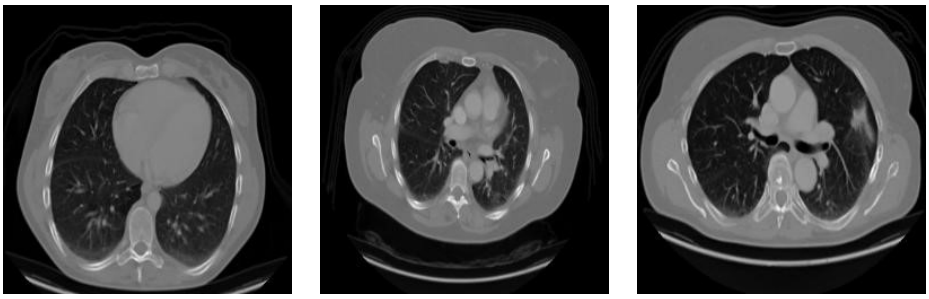

(a) (b) (c)

Figure 9:. Pre-processed images using PPT-MF technique over existing techniques

Table 3: Pre-processing Analysis for bad weather case

Methods	PSNR (dB)	SSIM
Conventional MF	28.85271	0.897052
Mean filter	28.42375	0.846788
GF	32.40592	0.912735
PPT-MF	36.17652	0.939818

4.3 Segmentation Analysis

Fig. 10 displays the segmented images using modified Res U-Net over U-Net, Seg Net and Res U-Net. The segmented imageries attained with modified Res U-Net seems to show better ROI areas than extant methods. In modified Res U-Net, the whole structure of Res U-Net is altered for enhancing the segmentation performance. Moreover, the proposed residual block in modified Res U-Net is incorporated with new layers like BN, ELTU, Leaky ReLU instead of ReLU and conv 2D functions. The modified Res U-Net enhances the generalization ability and improves the efficacy of representing learning features at varied depth levels. This is further obvious from Table 4, where, high accuracy, dice and Jaccard scores are established using modified Res U-Net over U-Net, Seg Net and Res U-Net.

Original

Segnet

Res-U-Net

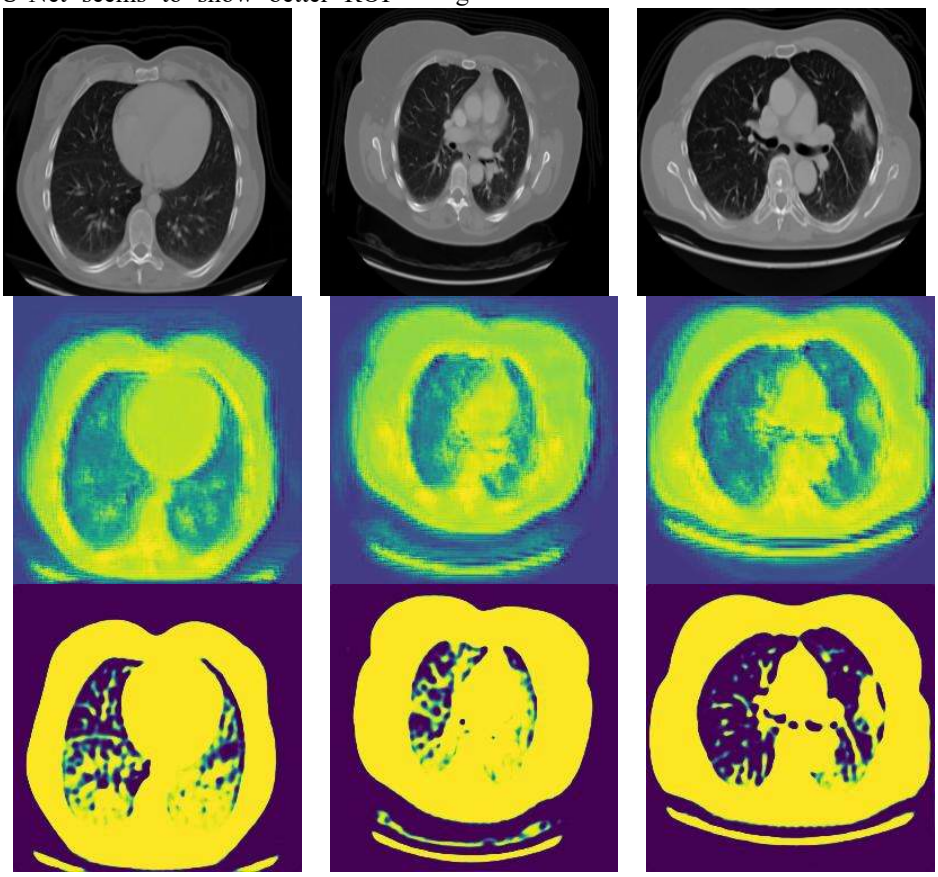

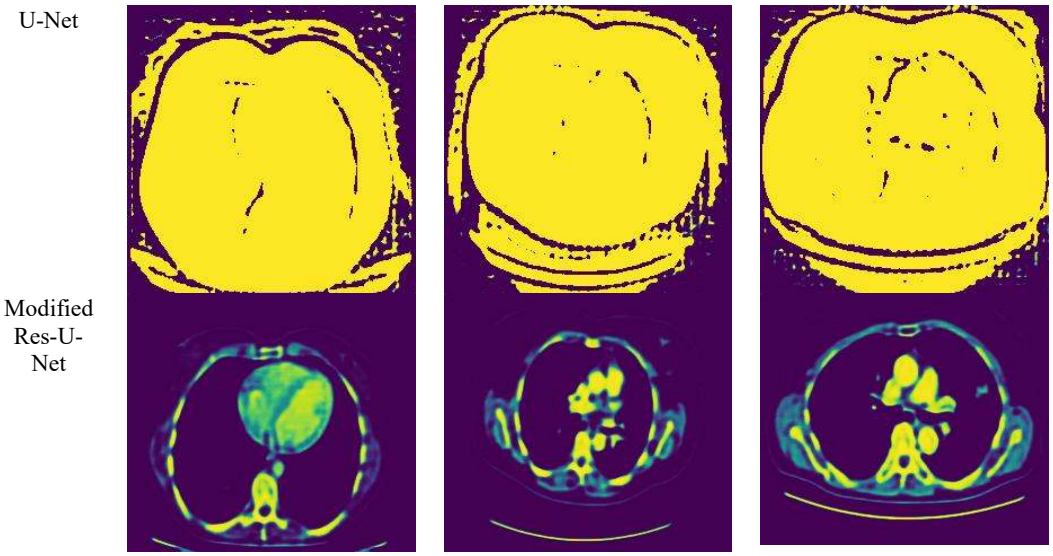

(a) (b) (c)

Figure 10: Depiction of segmented images (a) 1 (b) 2 (c) 3

Table 4: Segmentation Analysis using TL-MSNet

Metrics	U-Net	Seg Net	Res U-Net	Modified Res U-net
Accuracy	0.770099	0.763655	0.874931	0.961533
Jaccard	0.731011	0.722652	0.857681	0.949017
Dice	0.746217	0.737752	0.868937	0.914802

4.4 Performance Analysis

The analysis of developed LCC method deploying TL-MSNet over conventional classifiers is revealed in Fig. 11, 12, and 13. From the obtained results, TL-MSNet accomplishes better outcomes than shuffle net, Lenet, squeeze net, link net, alexnet, EfficientNet [9], ResNet, LeNet and DenseNet [37] for LCC. This work employs TL-based Modified Shufflenet, where, the TL-MSNet framework to be tested is allocated with pre-trained MSNet weights. In addition, a new modified SNet is proposed with diverse alterations. Particularly, the AP-RBN technique leads the network in light weighted path. Moreover, it sustains a better balancing among the accuracy and running speed of the network. The computing intricacy of the existing SNet model is also reduced using proposed TL-MSNet. The FPR outcomes further demonstrated the enhancement, as TL-MSNet attains a less score of 2%. In contrast, shuffle net, Lenet, squeeze net, link net, alexnet, EfficientNet [9] and DenseNet [37] have high FPR. The outcomes, thus establish the improvement of proposed TL-MSNet.

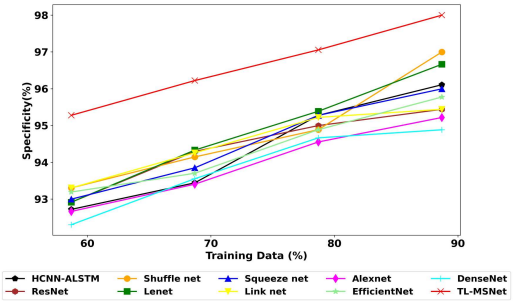

(a)

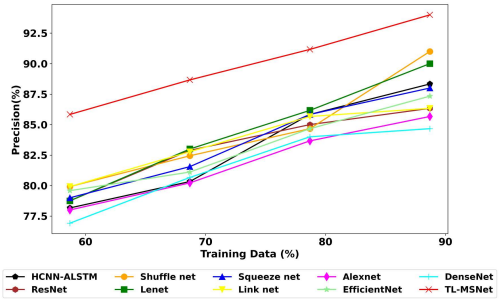

(b)

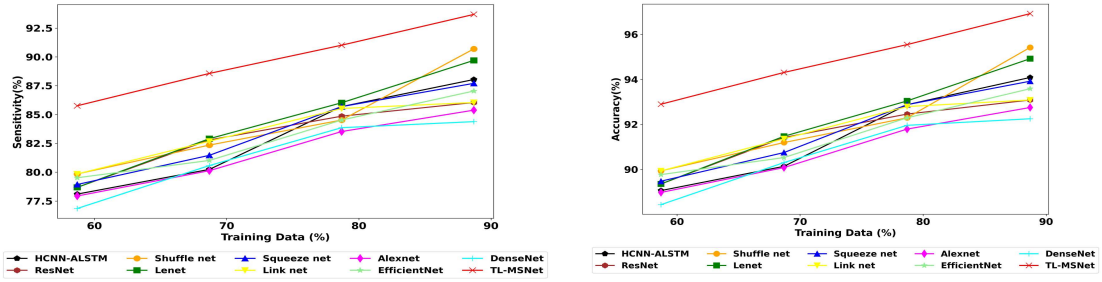

(c) (d)

Figure 11: Performance analysis of TL-MSNet over conventional classifiers on (a) Specificity (b) Precision (c) Sensitivity (d) Accuracy

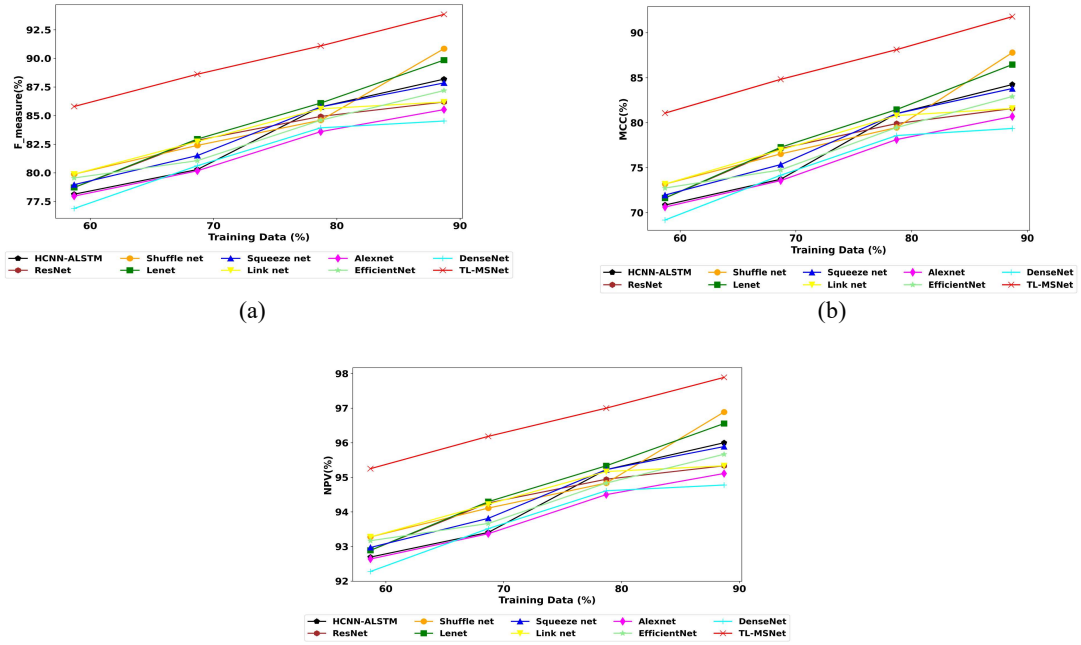

(a) (b)

(c)

Figure 12: Performance analysis of TL-MSNet over conventional classifiers on (a) F measure (b) MCC (c) NPV

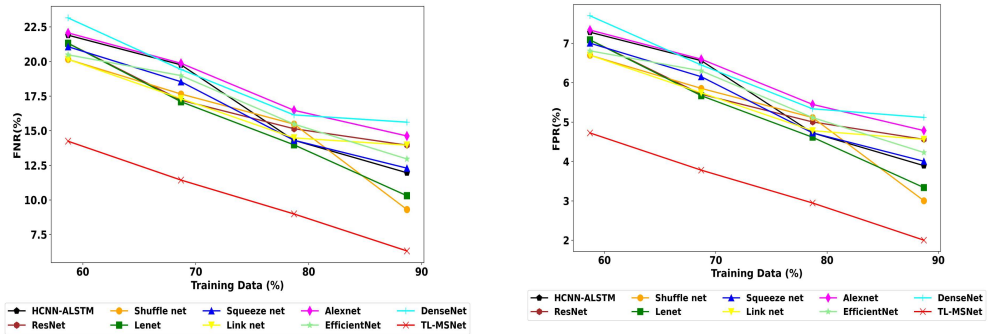

(a) (b)

Figure 13: Performance analysis of TL-MSNet over conventional classifiers on (a) FNR (b) FPR

4.5 Ablation Analysis on performance

Table 5 presents a comprehensive comparison of the proposed lung cancer classification framework under different configurations and against conventional machine learning classifiers. The fully proposed model achieves the best overall performance, recording the highest accuracy (0.9430), sensitivity (0.8856), specificity (0.9622), precision (0.8866), F-measure (0.8861), MCC (0.8482), and NPV (0.9618), while also yielding the lowest FPR (0.0377) and FNR (0.1143). Models without transfer learning and those using traditional classifiers such as MLP, SVM, and RF show reduced performance, indicating the advantage of the proposed deep learning-based approach. Additionally, variants employing conventional preprocessing, standard ResU-Net, conventional MRELBP, or excluding segmentation and feature extraction demonstrate noticeable drops across all metrics, highlighting the critical contribution of each module in the framework.

Table 5: Comparative Performance on Ablation Study Analysis

	Proposed without transfer learning	MLP	SVM	RF	Proposed with conventional preprocessing	Proposed with conventional ResUnet	Proposed with conventional MRELBP	Proposed without segmentation	Proposed without feature extraction	Proposed
Accuracy	0.9306	0.9174	0.9225	0.9181	0.9066	0.9182	0.9137	0.8870	0.8903	0.9430
Sensitivity	0.8609	0.8343	0.8446	0.8357	0.8130	0.8362	0.8271	0.7739	0.7803	0.8856
Specificity	0.9539	0.9451	0.9485	0.9456	0.9378	0.9456	0.9426	0.9248	0.9269	0.9622
Precision	0.8618	0.8355	0.8458	0.8369	0.813	0.8370	0.8279	0.7745	0.7810	0.8866
F_measure	0.8614	0.8349	0.8452	0.8363	0.813	0.8366	0.8275	0.7742	0.7807	0.8861
MCC	0.8152	0.7799	0.7936	0.7817	0.751	0.7821	0.7699	0.6989	0.7075	0.8482
NPV	0.9536	0.9447	0.9481	0.9451	0.9376	0.9453	0.9423	0.9245	0.9267	0.9618
FPR	0.0460	0.0548	0.0514	0.0543	0.0621	0.0543	0.0573	0.0751	0.0730	0.0377
FNR	0.1390	0.1656	0.1553	0.1642	0.1869	0.1637	0.1728	0.2260	0.2196	0.1143

4.6 Statistical analysis

The statistical study on accuracy by means of TL-MSNet over existing classifiers is exposed in Table 6. The analysis portrays the betterment of TL-MSNet over shuffle net, Lenet, squeeze net, link net, alexnet, EfficientNet [9] and DenseNet [37]. A higher accuracy of 0.949 is achieved for mean case by TL-MSNet, while, shuffle net, Lenet, squeeze net, link net, alexnet, EfficientNet [9] and DenseNet [37] achieves lesser accuracy of 0.9221, 0.9219, 0.91755, 0.91793, 0.90901, 0.915434 and 0.907378 correspondingly. Likewise, a high accuracy of 0.969 is achieved for max case by TL-MSNet, while, shuffle net, Lenet, squeeze net, link net, alexnet, EfficientNet [9] and DenseNet [37] scores smaller accuracies. The TL-MSNet overcomes the computing complexity issues and accuracy issues in existing SNet. Also, it sustains a better balancing among the accuracy and running speed of the network, making it better for LCC.

Table 6: *Statistical study of LCC using TL-MSNet over Existing classifiers*

Methods	Min	Max	Mean	Median	SD
Shufflenet	0.899375	0.954167	0.922101	0.917431	0.020361
Lenet	0.893542	0.949167	0.921962	0.922569	0.020443
Squeezenet	0.894792	0.939167	0.917552	0.918125	0.017404
Linknet	0.899375	0.930833	0.917934	0.920764	0.012542
Alexnet	0.889792	0.9275	0.90901	0.909375	0.014641
Efficient Net [9]	0.897708	0.935833	0.915434	0.914097	0.014912
Dense Net [37]	0.884375	0.9225	0.907378	0.911319	0.015211
TL-MSNet	0.928958	0.969167	0.949149	0.949236	0.014873

4.7 Analysis on varied Learning Rates

The analysis on varied LRs is given in Table 7 for proposed TL-MSNet. The LR is varied from 0.1, 0.01, 0.05 and 0.001. For all LRs, the proposed TL-MSNet attains higher accuracies above 90%. However, the proposed TL-MSNet shows utmost betterment when TD=90%.

Table 7: Analysis on varied LRs using TL-MSNet with respect to varied TDs

TD	LR= 0.1	LR = 0.01	LR = 0.05	LR = 0.001
60	0.925267	0.926782	0.927419	0.928958
70	0.938948	0.93939	0.941742	0.943056
80	0.95207	0.953129	0.954413	0.955417
90	0.963138	0.965276	0.967199	0.969167

4.8 Analysis of Confidence Interval

Table 8 summarizes the confidence intervals (lower and upper bounds) of performance for different classifiers, highlighting the stability and reliability of each model. Conventional deep learning architectures such as AlexNet, DenseNet, ResNet, LeNet, SqueezeNet, LinkNet, and EfficientNet

exhibit confidence intervals mostly ranging between 0.89 and 0.93, indicating moderate and consistent classification performance. ShuffleNet and HCNN-ALSTM demonstrate slightly improved bounds, with upper limits reaching 0.9436 and 0.9317, respectively, reflecting better generalization compared to other baseline models. Notably, the proposed TL-MSNet achieves the widest and highest confidence interval, spanning from 0.9324 to 0.9622, which confirms not only superior accuracy but also higher robustness and statistical reliability.

Table 8: Confidence Interval Analysis

Classifiers	Lower Bound	Upper Bound
HCNN-ALSTM	0.8933	0.9317
ResNet	0.8986	0.9251
Shuffle net	0.9052	0.9436
Lenet	0.8988	0.9397
Squeeze net	0.8979	0.9313
Link net	0.9029	0.9293
Alexnet	0.8925	0.9227
EfficientNet	0.8996	0.9293
DenseNet	0.8890	0.9176
TL-MSNet	0.9324	0.9622

4.9 Cross-Dataset Validation Performance Analysis

Table 9 illustrates the performance of the proposed model under cross-dataset validation by training on one database and testing on the other. When trained on db1 and tested on db2, the model achieves an accuracy of 0.9490, sensitivity of 0.8972, and specificity of 0.9663, indicating strong generalization capability. A slight performance improvement is observed when training on db2 and testing on db1, with accuracy increasing to 0.9561, sensitivity to 0.9112, and specificity to 0.9710. Similarly, precision, F-measure, MCC, and NPV show consistent gains in the second configuration, while error rates decrease, as reflected by lower FPR (0.0289) and FNR (0.0887). Overall, the results demonstrate that the proposed framework maintains high robustness and stability across different datasets, confirming its effectiveness and generalizability for lung cancer classification in heterogeneous data environments.

Table 9: Cross Validation of Analysis

Metrics	Cross Validation (train db1 test db2)	Cross Validation (train db2 test db1)
Accuracy	0.9490	0.9561
Sensitivity	0.8972	0.9112
Specificity	0.9663	0.9710
Precision	0.8991	0.9133
F_measure	0.8982	0.9123
MCC	0.8642	0.8830
NPV	0.96569	0.9703
FPR	0.03362	0.0289
FNR	0.10275	0.0887

4.10 Analysis of K- fold Validation

Table 10 presents a comparative analysis of classification performance across different values of K (from 2 to 6) for various deep learning models. Overall, most classifiers demonstrate a gradual improvement in performance as the value of K increases, indicating enhanced robustness with higher neighborhood or fold settings. Notably, the proposed TL-MSNet consistently outperforms all competing methods across all K settings, starting from 0.9464 at K = 2 and reaching a peak value of 0.9689 at K = 6. This consistent superiority highlights the effectiveness of the transfer learning strategy combined with the modified ShuffleNet architecture, demonstrating enhanced stability, generalization capability, and classification accuracy under varying K configurations.

Table 10: K fold validation Analysis of various classifiers

Classifiers	K=2	K=3	K=4	K=5	K=6
HCNN-ALSTM	0.8880	0.8995	0.8996	0.9363	0.9427
ResNet	0.8905	0.9020	0.9099	0.9135	0.9165
Shuffle net	0.8945	0.8947	0.9072	0.9267	0.9439
Lenet	0.9048	0.9108	0.9115	0.9117	0.9443
Squeeze net	0.8880	0.9034	0.9150	0.9198	0.9420
Link net	0.8977	0.8992	0.9107	0.9139	0.9253
Alexnet	0.8913	0.8934	0.9034	0.9046	0.9060
EfficientNet	0.9016	0.9164	0.9215	0.9317	0.9343
DenseNet	0.8816	0.8923	0.8980	0.9030	0.9230
TL-MSNet	0.9464	0.9583	0.9596	0.9606	0.9689

4.11 Training and Validation Accuracy vs Epochs

The training and validation accuracy curves in figure 14 demonstrate the learning behavior of the proposed model over 50 epochs, with accuracy values ranging from 0.65 to 1.00. At the initial epochs, both training and validation accuracies start near 0.65, indicating random initialization and limited feature learning. As the number of epochs increases, a steady improvement is observed, reflecting effective feature extraction and optimization. The training accuracy rises more rapidly and gradually converges close to 1.00, while the validation accuracy follows a similar trend with a slightly lower slope, confirming good generalization and minimal overfitting. After approximately 35–40 epochs, both curves stabilize, showing convergence and training saturation.

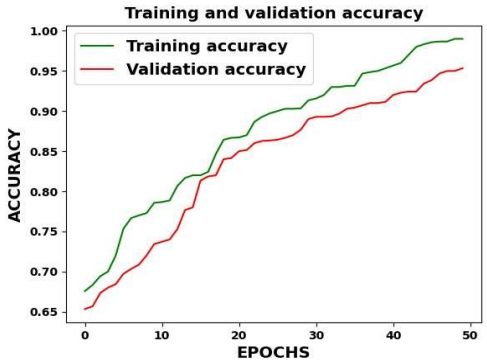

Figure 14: Training and Validation Accuracy

4.12 Statistical Significance Analysis Using T-Test (p-Values)

Table 11 presents the statistical significance of different classifiers evaluated using the T-test p-values. Lower p-values indicate stronger evidence that the observed performance differences are statistically significant. Among the evaluated models, DenseNet (0.01448) and AlexNet (0.01578) exhibit the lowest p-values, confirming statistically significant performance differences at the 5% significance level. ResNet (0.0305), LinkNet (0.03203), and EfficientNet (0.03230) also demonstrate significant results with p-values below 0.05. Overall, the analysis highlights that several deep learning models achieve statistically meaningful improvements, validating the reliability of the comparative evaluation.

Table 11: Analysis of Statistical T Test

Classifiers	T test pvalue
HCNN-ALSTM	0.0587
ResNet	0.0305
Shuffle Net	0.1119
Lenet	0.11180
Squeeze Net	0.05398
Link Net	0.03203
Alex Net	0.01578
Efficient Net	0.03230
Dense Net	0.01448

4.13 Confusion Matrix

Fig. 15 displays the confusion matrix, which assists in assessing the classification efficacy of the proposed classifier. It comprises the TP, FN, TN and FP values. The columns in the matrix signifies the cases, which are predicted by the classifier for a particular class, while, the rows of matrix signify the actual values belonging to that class. Here, proposed TL-MSNet effectually classifies 4 classes such as "normal, adenocarcinoma, large cell carcinoma, squamous cell carcinoma".

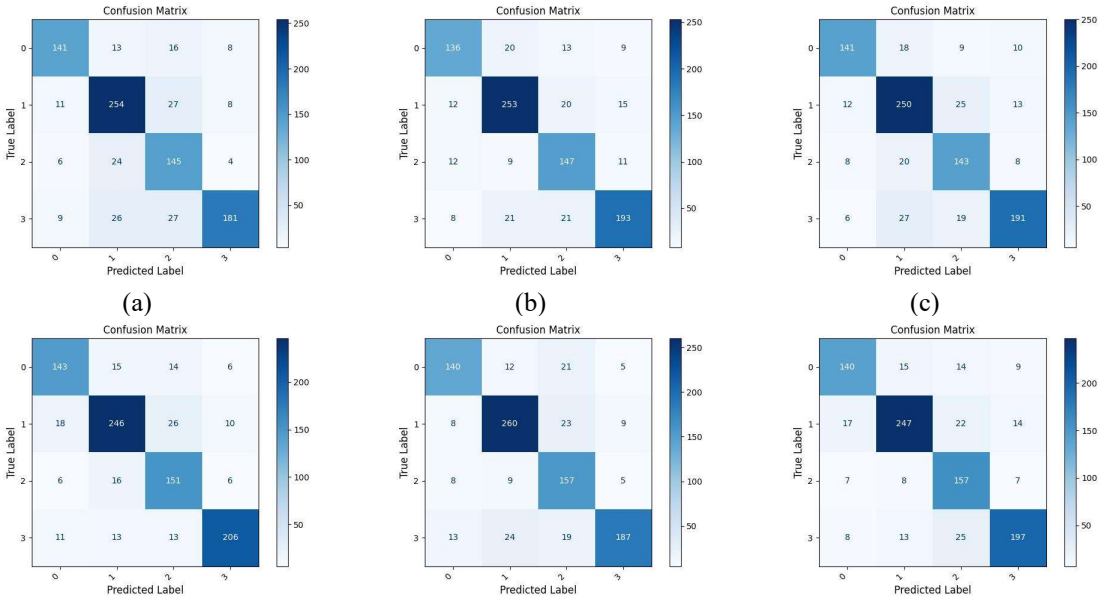

(a) (b) (c)

(d) (e) (f)

(g) (h)

Figure 15: Confusion matrix using proposed classifier and conventional classifiers namely (a) Alexnet (b) Efficient net (c) Dense net (d) Lenet (e) Linknet (f) Shuffle net (g) Squeeze net and (h) TL-MSNet

4.14 Analysis of ROC-AUC

Figure 16 shows the ROC-AUC graph depicts the relationship between the True Positive Rate (TPR), ranging from 0.0 to 1.0, and the False Positive Rate (FPR), also ranging from 0.0 to 1.0, for the proposed lung cancer classification model. Each curve represents the model's ability to distinguish between classes at various decision thresholds, where a higher TPR indicates more correct positive predictions and a lower FPR reflects fewer incorrect positive predictions. The area under the curve (AUC) quantifies overall discriminative performance, with values closer to 1.0 indicating superior classification capability. This confirms the model's robustness and reliability in correctly identifying lung cancer types while minimizing misclassification.

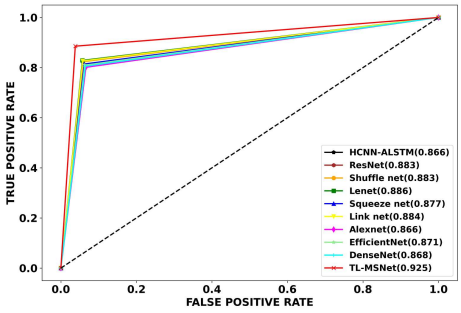

Figure 16: ROC-AUC Curve Analysis

4.15 Computational Complexity Analysis Using FLOPS

Table 12 compares the computational complexity of various classifiers in terms of floating-point operations per second (FLOPS). Among the evaluated models, LeNet exhibits the lowest computational cost with 3.43 G FLOPS, making it highly lightweight but potentially limited in representational capacity. ResNet (8.03 G) and the proposed TL-MSNet (9.2 G) demonstrate a favorable balance between computational efficiency and model complexity, indicating their suitability for resource-constrained environments. Overall, the proposed TL-MSNet achieves competitive computational efficiency with relatively low FLOPS while maintaining high classification performance, making it well-suited for real-time lung cancer classification in Cloud-IoT environments.

Table 12: Analysis Using FLOPS

Classifiers	FLOPS(G)
HCNN-ALSTM	14.2
ResNet	8.03
Shuffle Net	15.1
Lenet	3.43
Squeeze net	16.8
Link Net	10.6
Alex Net	25.9
EfficientNet	12.6
DenseNet	19
TL-MSNet	9.2

5. CONCLUSION

This research was made to classify LC using CT imageries. For classifying LC, the data were acquired from Cloud-IoT. The acquired data was stored in blockchain to ensure its security. After acquiring the data, the LCC process began by pre-processing the CT images using PPT-MF technique. Then, modified Res U-Net was USED for segmenting the lung images. Subsequently, features namely, Modified MRELBP, LMP, and PHOG were derived. After that, data augmentation was carried out using random sampling technique. Finally, classification was done using TL-MSNet model. From the analysis, a higher accuracy of 0.949 was achieved by TL-MSNet, while, shuffle net, Lenet, squeeze net, link net, alexnet, EfficientNet and DenseNet achieved less accuracy

of 0.9221, 0.9219, 0.91755, 0.91793, 0.90901, 0.915434 and 0.907378. In future, feature selection methods can be used for better classification.

REFERENCES

[1] Y. Chen, Y. Wang, F. Hu, L. Feng, T. Zhou, and C. Zheng, "LDNNET: Towards robust classification of lung nodule and cancer using lung dense neural network," *IEEE Access*, vol. 9, pp. 50301–50320, 2021.

[2] M. Hammad, M. ElAffendi, M. Asim, A. A. Abd El-Latif, and R. Hashiesh, "Automated lung cancer detection using novel genetic TPOT feature optimization with deep learning techniques," *Results in Engineering*, vol. 24, p. 103448, 2024.

[3] H. Yu, Z. Zhou, and Q. Wang, "Deep learning assisted predict of lung cancer on computed tomography images using the adaptive hierarchical heuristic mathematical model," *IEEE Access*, vol. 8, pp. 86400–86410, 2020.

[4] I. Nazir, I. U. Haq, M. M. Khan, M. B. Qureshi, H. Ullah, and S. Butt, "Efficient pre-processing and segmentation for lung cancer detection using fused CT images," Electronics, vol. 11, no. 1, p. 34, 2021.

[5] U. Muñoz-Aseguinolaza, I. Fernandez-Iriondo, I. Rodríguez-Moreno, N. Aginako, and B. Sierra, "Convolutional neural network-based classification and monitoring models for lung cancer detection: 3D perspective approach," Heliyon, vol. 9, no. 11, 2023.

[6] N. Y. Gharaibeh, R. De Fazio, B. Al-Naami, A. R. Al-Hinnawi, and P. Visconti, "Automated lung cancer diagnosis applying Butterworth filtering, bi-level feature extraction, and sparse convolutional neural network to LUNA16 CT images," Journal of Imaging, vol. 10, no. 7, p. 168, 2024.

[7] M. P. Paing, K. Hamamoto, S. Tungjitkusolmun, and C. Pintavirooj, "Automatic detection and staging of lung tumors using locational features and double-staged classifications," Applied Sciences, vol. 9, no. 11, p. 2329, 2019.

[8] K. K. Thanammal, "Lung cancer detection via deep learning-based pyramid network with honey badger algorithm," Measurement: Sensors, vol. 31, p. 100993, 2024.

[9] R. Raza, F. Zulfiqar, M. O. Khan, M. Arif, A. Alvi, M. A. Iftikhar, and T. Alam, "Lung-EffNet: Lung cancer classification using EfficientNet from CT-scan images," Engineering Applications of Artificial Intelligence, vol. 126, p. 106902, 2023.

[10] K. J. Eldho and S. Nithyanandh, "Lung cancer detection and severity analysis with a 3D deep learning CNN model using CT-DICOM clinical dataset," *Indian Journal of Science and Technology*, vol. 17, no. 10, pp. 899–910, 2024.

[11] A. Saha, S. M. Ganie, P. K. D. Pramanik, R. K. Yadav, S. Mallik, and Z. Zhao, "VER-Net: A hybrid transfer learning model for lung cancer detection using CT scan images," *BMC Medical Imaging*, vol. 24, no. 1, p. 120, 2024.

[12] A. Gopinath, P. Gowthaman, M. Venkatachalam, and M. Saroja, "Computer aided model for lung cancer classification using cat optimized convolutional neural networks," *Measurement: Sensors*, vol. 30, p. 100932, 2023.

[13] L. Wang, C. Zhang, Y. Zhang, and J. Li, "An automated diagnosis method for lung cancer target detection and subtype classification-based CT scans," *Bioengineering*, vol. 11, no. 8, p. 767, 2024.

[14] E. S. M. Elkenawy, A. A. Alhussan, D. S. Khafaga, Z. Tarek, and A. M. Elshewey, "Greylag goose optimization and multilayer perceptron for enhancing lung cancer classification," *Scientific Reports*, vol. 14, no. 1, p. 23784, 2024.

[15] B. Ar and V. K. R. S., "A deep learning-based lung cancer classification of CT images using augmented convolutional neural networks," *ELCVIA*, vol. 21, no. 1, pp. 130–142, 2022.

[16] S. R. R. B., S. Sen, R. Bhatt, M. L. Dhanetwal, M. Sharma, and R. Naaz, "Stacked neural nets for increased accuracy on classification on lung cancer," *Measurement: Sensors*, vol. 32, p. 101052, 2024.

[17] S. J. Shabu, J. Refonaa, S. Mallik, D. Dhamodaran, L. J. Grace, A. Ksibi, and T. A. N. Alshalali, "An improved adaptive neuro-fuzzy inference framework for lung cancer detection and prediction on Internet of Medical Things platform," *International Journal of Computational Intelligence Systems*, vol. 17, no. 1, p. 228, 2024.

[18] I. Bhatia, Aarti, S. I. Ansarullah, F. Amin, and A. Alabrah, "An advanced lung carcinoma prediction and risk screening model using transfer learning," *Diagnostics*, vol. 14, no. 13, p. 1378, 2024.

[19] A. Masood, P. Yang, B. Sheng, H. Li, P. Li, J. Qin, and D. D. Feng, "Cloud-based automated clinical decision support system for detection and diagnosis of lung cancer in chest CT," *IEEE Journal of Translational Engineering in Health and Medicine*, vol. 8, pp. 1–13, 2019.

[20] A. M. Harale, V. K. Bairagi, E. Boonchieng, and M. R. Bachute, "Nodules detection in lungs CT images using improved YOLOv5 and classification of types of nodules by CNN-SVM," *IEEE Access*, 2024.

[21] R. Mahum and A. S. Al-Salman, "Lung-RetinaNet: Lung cancer detection using a RetinaNet with multi-scale feature fusion and context module," *IEEE Access*, vol. 11, pp. 53850–53861, 2023.

[22] N. Tawfik, H. M. Emara, W. El-Shafai, N. F. Soliman, A. D. Algarni, and F. E. Abd El-Samie, "Enhancing early detection of lung cancer through advanced image processing techniques and deep learning architectures for CT scans," *Computers, Materials and Continua*, vol. 81, no. 1, pp. 271–307, 2024.

[23] M. Ragab, I. Katib, S. A. Sharaf, F. Y. Assiri, D. Hamed, and A. A. M. Al-Ghamdi, "Self-upgraded cat mouse optimizer with machine learning driven lung cancer classification on computed tomography imaging," *IEEE Access*, vol. 11, pp. 107972–107981, 2023.

[24] A. Wehbe, S. Dellepiane, and I. Minetti, "Enhanced lung cancer detection and TNM staging using YOLOv8 and TNMClassifier: An integrated deep learning approach for CT imaging," *IEEE Access*, 2024.

[25] I. Naseer, S. Akram, T. Masood, M. Rashid, and A. Jaffar, "Lung cancer classification using modified U-Net based lobe segmentation and nodule detection," *IEEE Access*, vol. 11, pp. 60279–60291, 2023.

[26] H. K. Kalidindi and N. Srinivasu, "Deep ensemble model with blockchain technology for lung cancer detection with secured data sharing," Computational Biology and Chemistry, p. 108729, 2025

[27] S. Alam, S. Bhatia, M. Shuaib, M. M. Khubrani, F. Alfayez, A. A. Malibari, and S. Ahmad, "An overview of blockchain and IoT integration for secure and reliable health records monitoring," *Sustainability*, vol. 15, no. 7, p. 5660, 2023.

[28] H. S. A. Fang, T. H. Tan, Y. F. C. Tan, and C. J. M. Tan, "Blockchain personal health records: Systematic review," *Journal of Medical Internet Research*, vol. 23, no. 4, e25094, 2021.

[29] Y. Song and J. Liu, "An improved adaptive weighted median filter algorithm," in *Journal of Physics: Conference Series*, vol. 1187, no. 4, p. 042107, 2019.

[30] M. W. Sabir, Z. Khan, N. M. Saad, D. M. Khan, M. A. Al-Khasawneh, K. Perveen, and S. S. A. Ali, "Segmentation of liver tumor in CT scan using ResU-Net," *Applied Sciences*, vol. 12, no. 17, p. 8650, 2022.

[31] A. Saïdani and A. K. Echi, "Pyramid histogram of oriented gradient for machine-printed/handwritten and Arabic/Latin word discrimination," in *Proc. SoCPaR*, pp. 267–272, 2014.

[32] T. Mohammad and M. L. Ali, "Robust facial expression recognition based on local monotonic pattern (LMP)," in *Proc. ICCIT*, pp. 572–576, 2011.

[33] L. Liu, S. Lao, P. W. Fieguth, Y. Guo, X. Wang, and M. Pietikäinen, "Median robust extended local binary pattern for texture classification," *IEEE Transactions on Image Processing*, vol. 25, no. 3, pp. 1368–1381, 2016.

[34] E. Goceri, "Medical image data augmentation: Techniques, comparisons and interpretations," *Artificial Intelligence Review*, vol. 56, no. 11, pp. 12561–12605, 2023.

[35] S. Ying, Y. Sun, F. Zhou, and L. Lin, "ShuffleNet V2–3 stacked BiLSTM-based tool wear recognition model for turbine disc fir-tree slot broaching," *Machines*, vol. 11, no. 1, p. 92, 2023.

[36] Y. Zhou, C. Fu, Y. Zhai, J. Li, Z. Jin, and Y. Xu, "Identification of rice leaf disease using improved ShuffleNet V2," *Computers, Materials & Continua*, vol. 75, no. 2, 2023.

[37] Y. Zhou, C. Fu, Y. Zhai, J. Li, Z. Jin, and Y. Xu, "Identification of rice leaf disease using improved ShuffleNet V2," *Computers, Materials & Continua*, vol. 75, no. 2, 2023.

[38] Kaggle Dataset: Chest CT-Scan Images. https://www.kaggle.com/datasets/mohamedhanyyy/chest-ctscan-image